Proceedings of the 5th International Symposium- Supercritical CO2 Power Cycles

March 29-31, 2016, San Antonio, TX, USA

Paper No. 133

NUMERICAL INVESTIGATION OF POTENTIAL EROSION MECHANISMS IN TURBULENT FLOW OF SCO2 PIPE BENDS

Sourabh V. Apte
School of Mechanical, Industrial and
Manufacturing Engineering
Oregon State University
Corvallis, Oregon 97331
Email: sva@oregonstate.edu

Ömer Doğan
National Energy Technology Laboratory
Albany, Oregon 97321
Email: Omer.Dogan@NETL.DOE.GOV

Chaitanya Ghodke
School of Mechanical, Industrial and
Manufacturing Engineering
Oregon State University
Corvallis, Oregon 97331
Email: ghodkec@oregonstate.edu

ABSTRACT

Supercritical Carbon Dioxide (sCO_2) has been used for power generation cycles owing to its non-toxic, non-flammable properties and low cost. The high pressure ($\sim$ 200-350 bar) and high density fluid also enables extremely compact and high efficiency turbomachinery designs. Owing to high pressures and temperatures ($\sim 700^{\circ}$C); however, there is evidence that even for a fairly pure sCO_2 flowing through small pipe bends at high flow rates can lead to material erosion. It is hypothesized that erosion may occur due to large fluctuations in wall shear stresses and pressure owing to turbulence, secondary flow patterns, and property variations. To test this hypothesis, predictive large-eddy simulation (LES) of a single-phase, turbulent flow of sCO2 in a 90° pipe bend is performed at different Reynolds numbers (5000–27000) with and without heat transfer. The radius of curvature to pipe diameter ratio is varied between 1 and 3. First, the isothermal flow is validated against available experimental and numerical data for these flow conditions. Shear stress and pipe wall temperature statistics are computed at different cross-sections downstream of the pipe bend and their potential to cause pipe wall erosion is evaluated.

1 INTRODUCTION

Supercritical Carbon Dioxide (sCO_2) are being developed for power generation in thermal solar, fossil energy and nuclear power plants. It is an ideal working fluid for closed-loop power generation as it is non-toxic, non-flammable and low-cost fluid. The high pressures ($\sim$ 200-350 bar) and high density fluid enables extremely compact and high efficiency turbomachinery designs. Owing to high pressures and temperatures ($\sim$ 500-750°C); however, it is critical to address the compatibility and erosion resistance of materials used in these power generation cycles. For example, recent work at Sandia National Laboratory [1] indicates evidence of substantial erosion in the inlet nozzle and turbine blades. It is conjectured that small metal particles and impurities in sCO_2 caused the corrosion and failure of the blades.

It is also possible that even a fairly pure sCO_2 flowing through small pipe bends or junctions causes erosion of the material. It is thus critical to identify potential sources of this erosion. For pure supercritical CO_2 flowing through pipe or duct bends, it is hypothesized that erosion may occur due to (i) large fluctuations in local temperature and pressure due to turbulence, secondary flow patterns, and property variations causing substantial shear stresses on the pipe walls, and (ii) surface or geometric irregularities impacting wall shear stresses and pressure variations.

To test these hypotheses and to gain better understanding of the stress distributions on the inner walls of pipe bends, predictive numerical simulation of a single-phase, turbulent flow with and without heat transfer in pipe bends at representative conditions and flow Reynolds numbers is performed in the present work. Considerable work exploring the dynamics of laminar and turbulent flow through pipe bends has been conducted [2–4]. Flow in curved pipes with bends involves flow turning that results in centrifugal forces on the fluid elements and corresponding pressure field to balance these forces. Formation of counter-rotating vortices, commonly termed as Dean vortices, are observed as the fluid elements with higher velocity are forced to the outside of the bend and lower velocity elements are forced toward the inside [2, 3]. These curvature-induced swirling motions and their strength is described in terms of the Dean number, De, where $De = \sqrt{D/2R_c}Re_D$. Here $Re_D = DU_b/\nu$ is the Reynolds number, D is the diameter of the pipe, R_c is the radius of curvature of the bend measured to the pipe centerline, U_b is the bulk velocity, and ν is the kinematic viscosity of the fluid. The unsteady behavior of Dean vortices and the time-scales related to oscillations of these vortices, reattachment point after the bend, and resultant variations in the shear stresses on the walls in turbulent flow has not been investigated thoroughly. Rutten *et al.* [3] investigated turbulent flows in a 90° pipe bend using large-eddy simulations at Reynolds numbers of 5000–27000. Their work indicated that the overall forces on the pipe walls showed distinct peak in the power spectra of overall forces related to the vortex shedding at the inner side of the bend. At large Re_D, the power spectra also exhibited frequency of oscillation much lower than the vortex shedding from flow separation. This was attributed to two Dean vortices whose strength vary in time dominating the flowfield. This also suggests that local variation in the wall shear forces, especially after the bend, can be important in magnitude as well as time-scales. Such variations in local shear stresses may be relevant to the erosion problem, especially at very large Reynolds numbers.

In the present work, we explore the turbulent flow through a 90° bend to first validate our results against those available from experiments as well as other simulations, and then investigate the nature of shear force variations at different locations after the pipe bend. In addition, effect of thermal variations of properties of the fluid at large pressures and temperatures can be investigated to represent the application of sCO2 as the heat transfer fluid in thermal power plants.

2 MATHEMATICAL FORMULATION

In this section, the mathematical formulation for the single-phase LES with heat transfer are described. The mathematical formulation is based on the three-dimensional, variable density, low-Mach number equations for the fluid phase. Any acoustic interactions and compressibility effects are neglected. In addition, in writing the energy equation, we invoke the low-Mach number assumptions together. Also the viscous dissipation is assumed negligible. Radiative heat transfer is also neglected in this study. The Favre-averaged governing equations for LES of the zero-Mach number, variable density flow are given below,

$$\frac{\partial \overline{\rho_g}}{\partial t} + \frac{\partial \overline{\rho_g} \tilde{u_j}}{\partial x_j} = 0 \tag{1}$$

$$\frac{\partial \overline{\rho_g} \tilde{u_i}}{\partial t} + \frac{\partial \overline{\rho_g} \tilde{u_i} \tilde{u_j}}{\partial x_j} = -\frac{\partial \overline{p}}{\partial x_i} + \frac{\partial}{\partial x_j}\left(2\overline{\mu}\tilde{S_{ij}}\right) - \frac{\partial q^r_{ij}}{\partial x_j} \tag{2}$$

$$\frac{\partial \overline{\rho_g} \tilde{h}}{\partial t} + \frac{\partial \overline{\rho_g} \tilde{h} \tilde{u_j}}{\partial x_j} = \frac{\partial}{\partial x_j}\left(\overline{\rho_g}\tilde{\alpha_h}\frac{\partial \tilde{h}}{\partial x_j}\right) - \frac{\partial q^r_{hj}}{\partial x_j} \tag{3}$$

where

$$\tilde{S_{ij}} = \frac{1}{2}\left(\frac{\partial \tilde{u_i}}{\partial u_j} + \frac{\partial \tilde{u_j}}{\partial u_i}\right) - \frac{1}{3}\delta_{ij}\frac{\partial \tilde{u_k}}{\partial x_k}, \tag{4}$$

and $\tilde{\rho_g}$ is the density of the fluid, $\tilde{u_i}$ is the velocity, $\overline{\mu}$ is the viscosity, $\overline{p}$ is the pressure, and the total enthalpy $\tilde{h}$ is given as

$$\tilde{h} = \tilde{h}_{\text{ref}} + \int_{T_{\text{ref}}}^{T} C_p(T)dT \tag{5}$$

is the total enthalpy. In the limit of zero-Mach number assumption, the thermodynamic pressure field within the domain remains constant at some reference value (250 bar used for sCO2 calculations). The density of the fluid then is simply a function of the temperature, and an ideal gas-law is used in the present work. The fluid properties for supercritical CO2 vary with temperature and are considered in the calculations. The properties of sCO2 at 250 bar vary significantly over the range of 700-1300 K, the temperature range typically of interest in sCO2 heat exchangers. The property variations and the polynomial fits are given in figures 1a-d.

The subgrid scale unclosed transport terms in the momentum, scalar, and enthalpy equations are grouped into the residual stress q^r_{ij}, and residual flux of enthalpy q^r_{hj}. The dynamic Smagorinsky model by Moin et al. [5,6] is used. The dynamic model has no adjustable constants, and thus allows evaluation of the predictive capability of the model. The subgrid scale stress, q^r_{ij} is modeled as,

$$q^r_{ij} = \overline{\rho}(\tilde{u_i}\tilde{u_j} - \widetilde{u_i u_j}) = 2\mu_t \tilde{S}_{ij} - \frac{1}{3}\overline{\rho} q^2 \delta_{ij}, \tag{6}$$

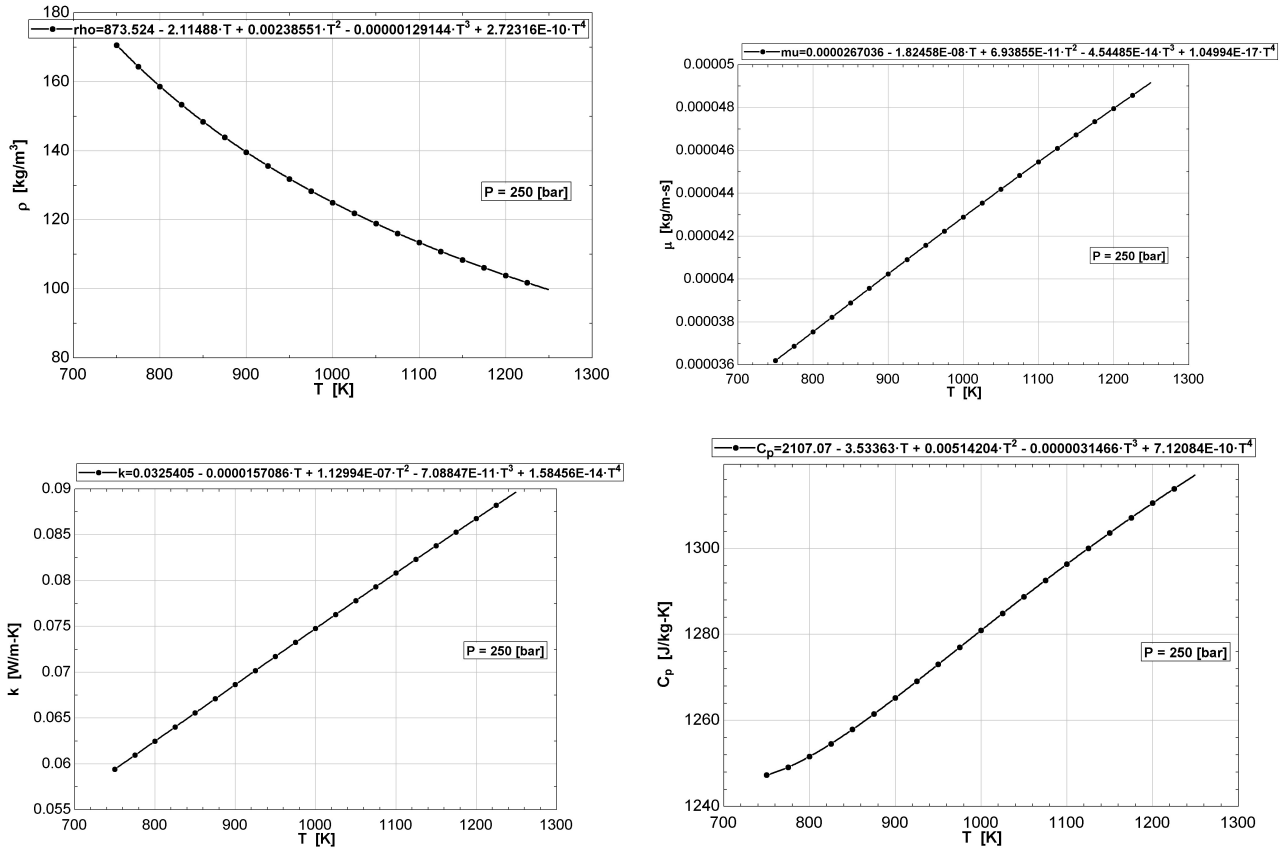

FIGURE 1: Variation of properties of sCO2 at 250 bar over the temperature range of 700-1300 K.

where the isotropic part of the subgrid stress q^2 is absorbed into the pressure term, and the subgrid viscosity mu_t is given as

$$\mu_t = C_\mu \overline{\rho}\overline{\Delta}^2 \sqrt{\widetilde{S_{ij}}\widetilde{S_{ij}}}. \tag{7}$$

Here, $\overline{\Delta}$ is the filter width and the coefficient C_μ is obtained using least-squares approach following the dynamic procedure [7]. Similarly, the subgrid scale term in the enthalpy equation is modeled as,

$$q^r_{hj} = \overline{\rho}(\tilde{h}\tilde{u}_j - \widetilde{hu}_j) = \overline{\rho}\alpha_t \frac{\partial \tilde{h}}{\partial x_j}, \tag{8}$$

where

$$\overline{\rho}\alpha_t = C_\alpha \overline{\rho}\overline{\Delta}^2 \sqrt{\widetilde{S_{ij}}\widetilde{S_{ij}}}, \tag{9}$$

and the coefficient C_α is also obtained using the dynamic procedure.

3 COMPUTATIONAL APPROACH and VALIDATION STUDY

An energy-conserving, finite-volume scheme for unstructured, arbitrarily shaped grid elements is used to solve the fluid-flow equations using a fractional step algorithm [5, 6, 8]. The velocity and pressure are stored at the centroids of the volumes. The cell-centered velocities are advanced in a predictor step such that the kinetic energy is conserved. The predicted velocities are interpolated to the faces and then projected. Projection yields the pressure potential at the cell-centers, and its gradient is used to correct the cell and face-normal velocities. A novel discretization scheme for the pressure gradient was developed by Mahesh *et al.* [5] to provide robustness *without numerical dissipation* on grids with rapidly varying elements. This algorithm was found to be imperative to perform LES at high Reynolds number in complex flows. The overall algorithm is second-order accurate in space and time for uniform orthogonal grids. A numerical solver based on this approach was developed and shown to give very good results for both simple [9] and complex geometries [6] and is used in the present study. A thorough verification and validation of the algorithm was conducted [10,11] to assess the accuracy of the numerical scheme for test cases involving two-dimensional decaying Taylor vortices, flow through a turbulent channel and duct flows [10] and particle-laden turbulent flows [6, 9].

3.1 Validation study

In order to verify and validate the solver for the specific case under investigation, heat transfer in the turbulent channel case is validated against the data of [12, 13]. As shown in Fig. 2, x, y and z are, respectively, the streamwise, wall-normal and spanwise directions and u, v and w are the velocity components in those directions. The computational domain, shown in Fig. 2, consists of a doubly periodic box (in x and z directions) with a smooth no-slip wall at $y = 0$ and at $y = H$, where H is the height of the channel. Based on [12], the in-plane domain length is 5π and 2π in the streamwise and spanwise directions, respectively. The Reynolds number Re_τ based on the wall friction velocity u_τ and $H/2$ is 180 and the Prandtl number is 1. As shown in Fig. 2 isothermal boundary conditions are imposed for the scalar field of ϕ. Total number of grid points used is $128 \times 96 \times 128$. Consistent with canonical channel flow and boundary layer studies, uniform grids are used in the streamwise and spanwise directions and grids are stretched in the wall-normal direction using a hyperbolic tangent function.

Figure 3 shows profiles of (a) mean and (b) *rms* fluctuations for the velocity field compared with [13]. In Fig. 3 (c) and (d), mean and *rms* fluctuations, respectively for the scalar (temperature) field are presented. Present data is typically in a good agreement with [13], especially the location of peak *rms* fluctuations away from the wall, thickness of boundary layer, etc. This suggests that the present solver is able to provide accurate descriptions of the turbulent flows with heat transfer. Note that, deviations in the data of scalar field away from the wall shown in Fig. 3 (c) and (d) are result of initialization of the scalar field and indicates that the simulation needs to be run longer. Nevertheless, near-wall processes of molecular and turbulent diffusion are captured really well as indicated by the current trends of the results.

4 COMPUTATIONAL SETUP

The computational setup used consists of a circular cross-section pipe with a 90° bend as shown in figure 4. The pipe consists of a straight section of length $8D_b$, followed by the bend section and another straight section of $8D_b$ length. Two different radii of curvatures are investigated, $R_c/D = 1$ and $R_c/D = 3$. Owing to the bend geoemetry an unstructured grid with predominantly hexagonal mesh is used for calculations.

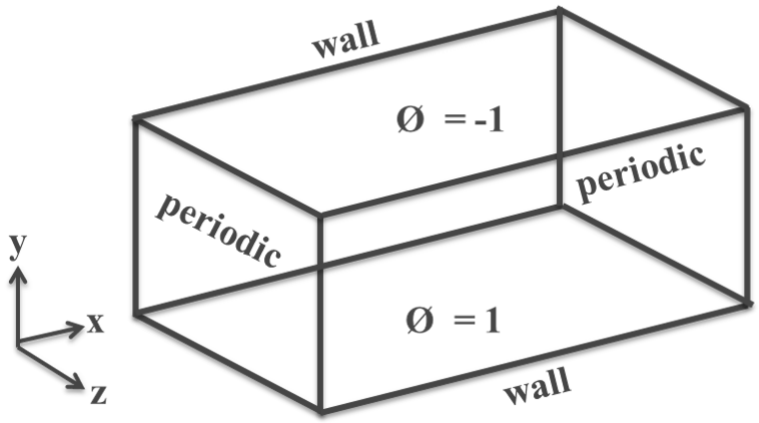

FIGURE 2: Computational domain and boundary conditions for validation of the flow solver for turbulent flow with heat transfer.

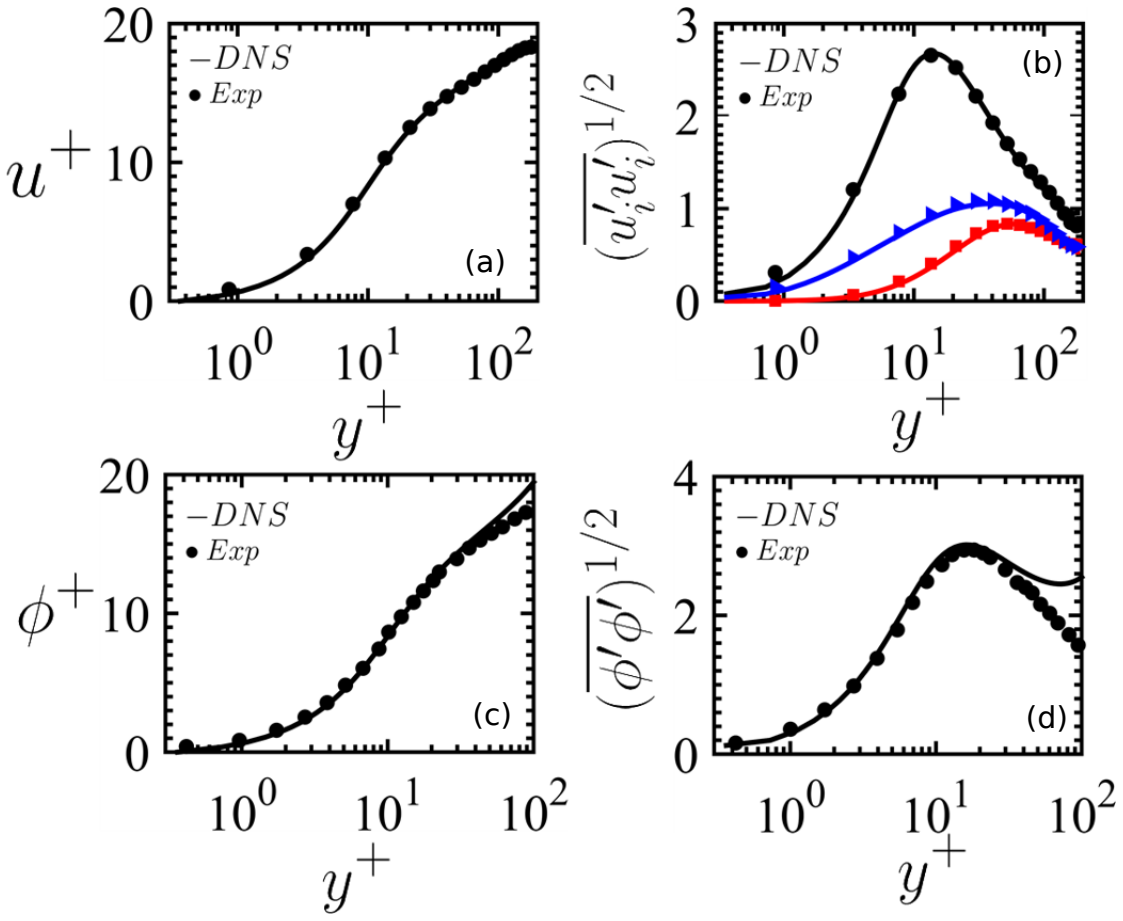

FIGURE 3: Comparison of the mean and rms profiles with experimental data [13]: (a) mean and (b) *rms* fluctuations of velocity; profiles of (c) mean and (d) *rms* fluctuations in temperature. Solid lines indicate present DNS results and symbols represent results from [13].

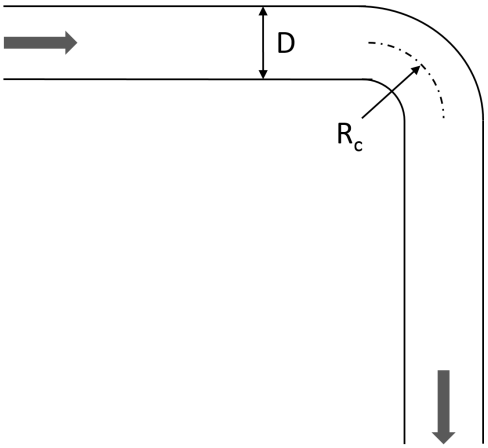

FIGURE 4: Schematic diagram of the computational setup for the 90° pipe bend. Two cases with $R_c/D = 1$ and 3 are simulated.

The flowfields simulated are for two different Reynolds numbers, $Re_D = 5300$ and $Re_D = 27,000$ similar to the work by Rutten *et.* [3]. The grid resolutions are determined by estimating the bulk velocity for a certain unit friction velocity (u_τ), using the Blassius law,

$$f = \frac{0.316}{Re_D^{0.25}} = 3\left(\frac{u_\tau}{U_b}\right)^2. \tag{10}$$

For the two Reynolds numbers, 5300 and 27000, are ratio of the friction velocity to the bulk velocity are 0.0683 and 0.05551, respectively. The corresponding turbulent Reynolds numbers, $Re_\tau = u_\tau D_b/\nu$, are 362 and 1500, respectively.

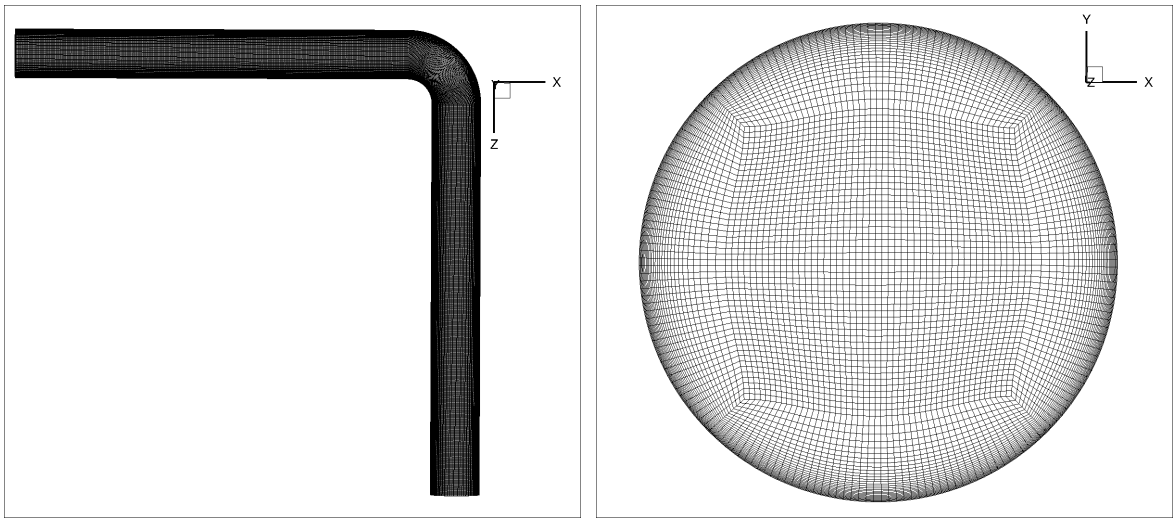

FIGURE 5: Computational mesh used for the pipe bend showing mostly hexagonal elements with minimal skewness.

Stretched grids are used in the wall normal direction with a minimum grid resolution near the wall in wall units of $\Delta r^+ \sim 0.8$ (see figure 5a,b). Nearly uniform grids are used in the axial direction with a resolution of $\Delta x^+ \sim 20$. The maximum resolution in the azimuthal direction is on the order of

$(r\Delta\theta)^+ \sim 20$. These resolutions are finer than those used by Rutten *et.* [3]. In the present wall-resolved large-eddy simulation, no-slip conditions are applied at walls. In LES, to create proper turbulence structure and velocity fluctuations, it is important to impose consistent fluctuations in the velocity field at the inlet [14]. Use of random fluctuations scaled with turbulence intensity values; however, can lead to convergence issues in a conservative numerical solver. A separate periodic pipe flow (length $8D_b$) is simulated at the desired mass-flow rate and Reynolds number using a body-force technique [14]. The velocity field obtained from this periodic pipe flow simulation is stored at a single plane every time-step and is used as the inlet condition for the pipe bend. This provides a fully developed, instantaneous, turbulent velocity profile at the inlet of the pipe bend. A convective outlet condition is enforced at the outlet. In this study, only an isothermal flowfield is simulated and thus effectsw of temperature and density variations and properties of sCO2 are not relevant. Later study involves turbulent flow with heat transfer where these effects do become important.

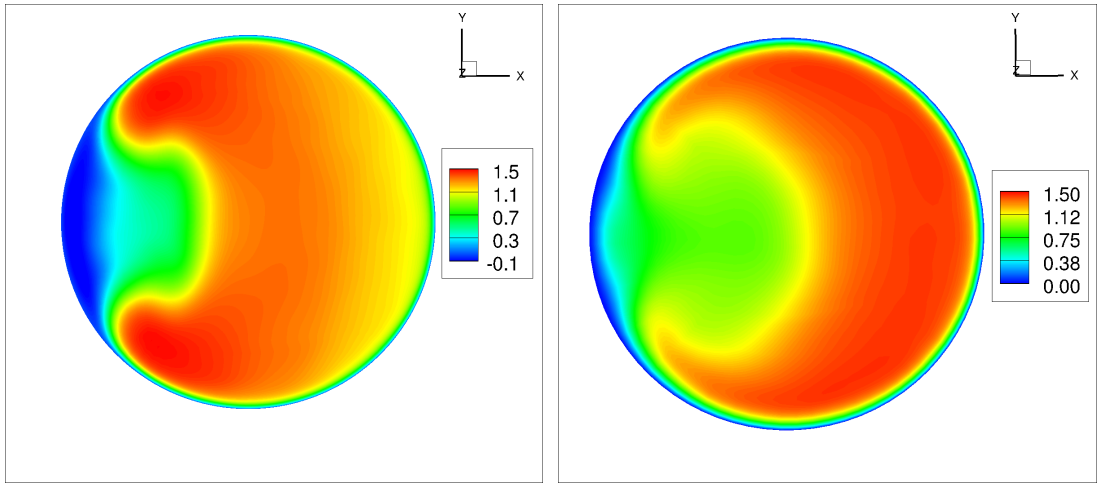

(a) $\frac{\overline{w}}{U_b}$ (b) $\frac{w_{rms}}{U_b}$

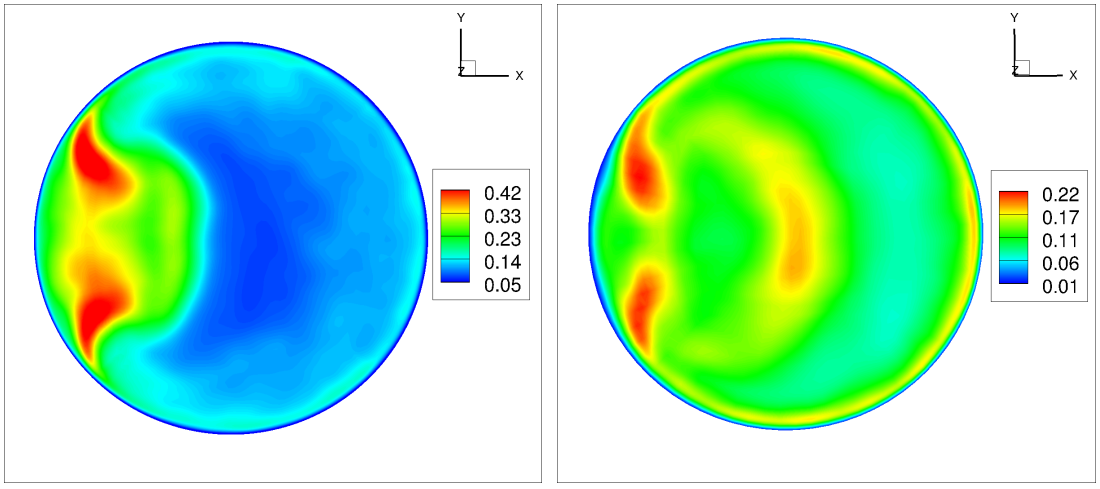

(c) $\frac{\overline{w}}{U_b}$ (d) $\frac{w_{rms}}{U_b}$

FIGURE 6: Contours of the mean and rms axial velocity for $R_c/D = 1$ (a,c) and $Re_D = 5300$ (b,d).

5 NUMERICAL RESULTS

The large-eddy simulation of $Re_D = 5300$ and $Re_D = 27000$ is carried out for several flow through times to obtain statistically stationary field. Both geometries with $R_c/D = 1$ and 3 are simulated. As the first step, we present the results for $Re_D = 5300$. At the entry to the bend, no centrifugal forces are present due to flow turning, but a radial pressure gradient results in a secondary flow towards the inner side of the bend. At the exit of the bend, a pair of counter-rotating vortices, the well-known Dean vortices, are present. For bend geometry with $R_c/D = 1$, strong curvature of the inner wall leads to flow separation. The separation and reattachments seem to move with time and this can lead to large changes in the shear and pressure forces on the bend walls. In addition, it is seen that stronger curvature for $R_c/D = 1$, leads to higher peaks in the rms velocity compared to those for $R_c/D = 3$. Figures 6a,b

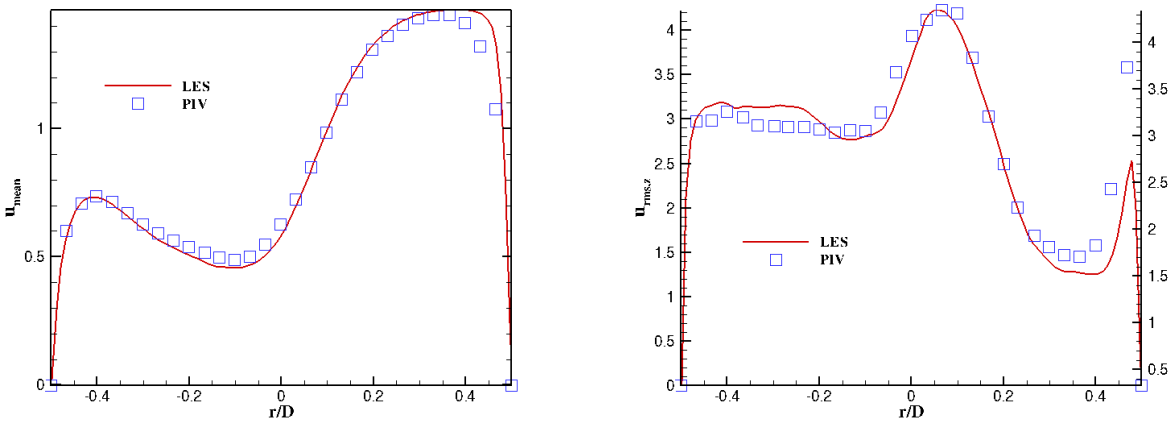

(a) $\frac{\overline{w}}{U_b}$ (b) $\frac{w_{rms}}{U_b}$

FIGURE 7: Radial variation of mean and rms axial velocity for $R_c/D = 1$ and $Re_D = 5300$ at $z/D = 1$. Symbols represent experimental data (PIV) [3, 15] and lines represent present LES simulation.

show the contour plots of mean axial velocity at $z/D = 1$ downstream of the bend for the two radii of curvatures, $R_c/D = 1$, and $R_c/D = 3$, respectively. The corresponding rms axial velocities are shown in Figures 6c,d. Figure 7 shows the radial variation of the mean and rms axial velocity at $z/D = 1$ for $R_c/D = 1$ case compared with the experimental data [15] and showing excellent agreement. Flow separation on the inner side of the bend results in lower axial velocities in the separation area and an accelerated flow at the outer side. It can be seen that the flow separation leads to stronger velocity fluctuations in the separation region compared to the outer region. A characteristic flow pattern with outward flow in the central part and inward flow near the bend walls is observed [3], confirming the accuracy of our simulations.

The total shear force on the bend walls is calculated for $R_c/D = 3$ and $Re_D = 5300$. Figure 8a shows the power spectra of normalized shear force versus the Strouhal number ($St = fD/U_b$). The time history of the normalized shear force is shown in figure 8b. It is observed that a low frequency peak is present at $St = 0.03$, which corresponds to frequency of approximately 0.5 Hz or a time scale of 2 s. Another peak is also observed at a $St = 0.1$, corresponding to a time scale of around 0.5 s. This suggests that the turbulent flow induces oscillations of bend wall shear forces which can have an effect on the wall erosion, especially if the force magnitudes are large. For heat exchangers, the operating conditions can lead to very large Reynolds numbers, and hence much higher shear forces. In addition, changes in temperatures and thermal properties of the fluid can influence the forces and their spectra as

well.

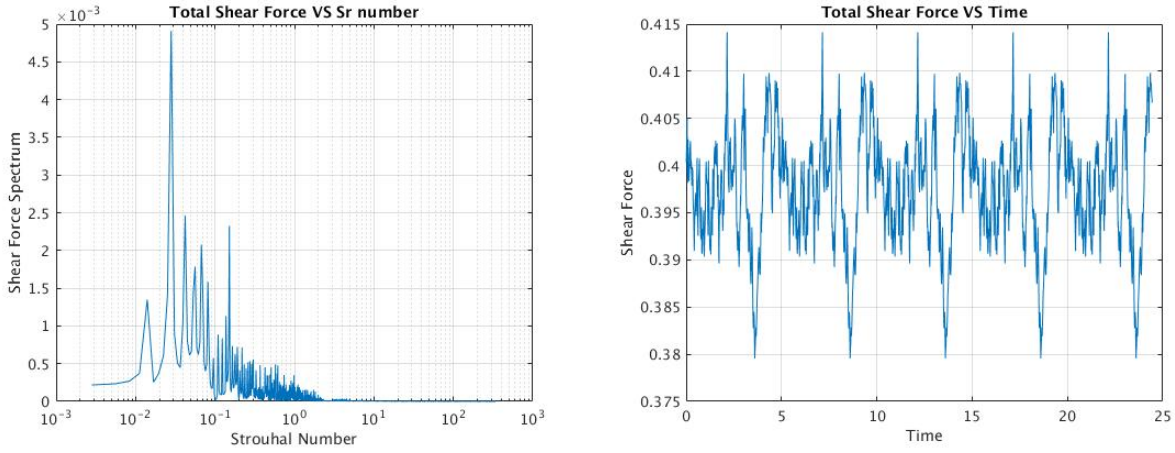

(a) (b)

FIGURE 8: Net normalized shear force on the pipe bend for $R_c/D = 3$ and $Re_D = 5300$: (a) Power spectra, (b) time series.

Considearble additional data on shear forces on pipe bend, instataneous variations of these forces, spectra of the forces as well as kinetic energy spectra are being processed at different Reynolds numbers. The goal is identify the magnitudes and time-scales associated with shear force variations after the bend and investigate the scaling of these forces with increasing flow rate (or Reynolds number). Finally, using instantaneous shear force variations an analysis of their effect on the bend material is to be investigated to evaluate their potential role in erosion mechanism.

6 Summary

Large eddy simulations of turbulent flow through 90° pipe bend with different radii of curvatures ($R_c/D = 1$, and 3) are performed using an unstructured grid solver based on the principles of energy conservation. Different Reynolds numbers 5000, 27,000 and 100,000 are simulated to understand the behavior of the flow field within the pipe bends, the dynamics of the Dean vortices, variations in the shear stress and pressure. Specifically, the goal is to obtain the magnitude and time scale of shear stress and pressure variations on the bend walls after the bend to identify their effects and potential role on erosion of the bend material. It is hypothesized that erosion may occur due to large fluctuations in wall shear stresses and pressure owing to turbulence, secondary flow patterns, and property variations. First, the isothermal flow is validated against available experimental and numerical data for these flow conditions, however, goal is to investigate flow of sCO2 with heat transfer representative of the flow conditions in modern heat exchangers. At present, a systematic validation study has been completed and presented in this work. This shows that the algorithm developed is capable of simulating variable density flows in complex geometries.

Acknowledgements

This work was performed in support of the U.S. Department of Energys Fossil Energy Advanced Combustion Program. The Research was executed through NETLs Research and Innovation Centers Advanced Combustion Field Work Proposal (Richard Dennis and Daniel Driscoll, Technology Managers and Briggs White, Project Monitor). This research was supported in part by an appointment (SA)

to the National Energy Technology Laboratory Research Participation Program sponsored by the U.S. Department of Energy and administered by the Oak Ridge Institute for Science and Education.

This report was prepared as an account of work sponsored by an agency of the United States Government. Neither the United States Government nor any agency thereof, nor any of their employees, makes any warranty, express or implied, or assumes any legal liability or responsibility for the accuracy, completeness, or usefulness of any information, apparatus, product, or process disclosed, or represents that its use would not infringe privately owned rights. Reference herein to any specific commercial product, process, or service by trade name, trademark, manufacturer, or otherwise does not necessarily constitute or imply its endorsement, recommendation, or favoring by the United States Government or any agency thereof. The views and opinions of authors expressed herein do not necessarily state or reflect those of the United States Government or any agency thereof.

REFERENCES

[1] Fleming, D., Kruizenga, A., Pasch, J., Conboy, T., and Carlson, M., 2014. "Corrosion and erosion behavior in supercritical co2 power cycles". In ASME Turbo Expo 2014: Turbine Technical Conference and Exposition, American Society of Mechanical Engineers, pp. V03BT36A002–V03BT36A002.

[2] Berger, S., Talbot, L., and Yao, L., 1983. "Flow in curved pipes". *Annual Review of Fluid Mechanics,* ***15***(1), pp. 461–512.

[3] Rütten, F., Schröder, W., and Meinke, M., 2005. "Large-eddy simulation of low frequency oscillations of the dean vortices in turbulent pipe bend flows". *Physics of Fluids (1994-present),* ***17***(3), p. 035107.

[4] Hellström, L. H., Zlatinov, M. B., Cao, G., and Smits, A. J., 2013. "Turbulent pipe flow downstream of a bend". *Journal of Fluid Mechanics,* ***735***, p. R7.

[5] Mahesh, K., Constantinescu, G., Apte, S., Iaccarino, G., Ham, F., and Moin, P., 2006. "Large-Eddy Simulation of Reacting Turbulent Flows in Complex Geometries". *Journal of Applied Mechanics,* ***73***, p. 374.

[6] Moin, P., and Apte, S., 2006. "Large-Eddy Simulation of Realistic Gas Turbine-Combustors". *AIAA journal,* ***44***(4), pp. 698–708.

[7] Germano, M., Piomelli, U., Moin, P., and Cabot, W., 1991. "A dynamic subgrid-scale eddy viscosity model". *Physics of Fluids A: Fluid Dynamics,* ***3***, p. 1760.

[8] Mahesh, K., Constantinescu, G., and Moin, P., 2004. "A numerical method for large-eddy simulation in complex geometries". *Journal of Computational Physics,* ***197***(1), pp. 215–240.

[9] Apte, S., Mahesh, K., Moin, P., and Oefelein, J., 2003. "Large-eddy simulation of swirling particle-laden flows in a coaxial-jet combustor". *International Journal of Multiphase Flow,* ***29***(8), pp. 1311–1331.

[10] Shams, E., Finn, J., and Apte, S., 2011. "A numerical scheme for euler–lagrange simulation of bubbly flows in complex systems". *International Journal for Numerical Methods in Fluids,* ***67***(12), pp. 1865–1898.

[11] Shams, E., and Apte, S. V., 2010. "Prediction of small-scale cavitation in a high speed flow over an open cavity using large-eddy simulation". *Journal of Fluids Engineering,* ***132***(11), p. 111301.

[12] Kasagi, N., Tomita, Y., and Kuroda, A., 1992. "Direct numerical simulation of passive scalar field in a turbulent channel flow". *J. Heat Transfer,* ***114***, pp. 598–606.

[13] Kawamura, H., Ohsaka, K., Abe, H., and Yamamoto, K., 1998. "Dns of turbulent heat transfer in channel flow with low to medium-high prandtl number field". *Intl. J. Heat and Fluid Flow,* ***19***, pp. 482–491.

[14] Pierce, C., and Moin, P., 1998. "Large eddy simulation of a confined coaxial jet with swirl and heat release". *AIAA Paper,* ***2892***.

[15] Brücker, C., 1998. "A time-recording dpiv-study of the swirl switching effect in a 90 bend flow". In Proceedings of the Eight International Symposium on Flow Visualization, Sorrento, Italy.